ELSEVIER

Carbohydrate Research 315 (1999) 76–88

CARBOHYDRATE RESEARCH

Conformational analysis of an α-galactosyl trisaccharide epitope involved in hyperacute rejection upon xenotransplantation

Jun Li, Mohamad B. Ksebati, Wei Zhang, Zhengmao Guo, Jianqiang Wang, Libing Yu, Jianwen Fang, Peng George Wang *

Department of Chemistry, Wayne State University, Detroit, MI 48202, USA

Received 8 October 1998; accepted 4 December 1998

Abstract

α-Galactosyl epitopes are carbohydrate structures bearing an α-Gal-(1→3)-Gal terminus (α-Gal epitopes). The interaction of these epitopes on the surface of animal cells with anti α-Gal antibodies in human serum is believed to be the main cause in antibody-mediated hyperacute rejection in xenotransplantation. In this paper, conformational analysis of an *N*-linked α-D-Gal*p*-(1→3)-β-D-Gal*p*-(1→4)-β-D-Glc*p* trisaccharide epitope was conducted in terms of each monosaccharide residue conformation, primary hydroxymethyl group configuration, and interglycosidic conformations. Selective 2D *J*-δ INEPT experiments have been carried out at three different temperatures to evaluate three-bond, long-range $^{13}C-^{1}H$ coupling constants for the crucial α-(1→3) linkage. The NMR experimental data were complemented by theoretical calculations. The flexibility and dynamics of the trisaccharide have been studied by Metropolis Monte Carlo simulations. Ensemble-averaged three-bond, long-range $^{13}C-^{1}H$ coupling constants and nuclear Overhauser effects were in good agreement with the experimental data. The α-(1→3) glycosidic linkage has shown a restricted flexibility as indicated by NMR spectroscopy and molecular modeling.

Keywords: α-Galactosyl epitopes; Xenotransplantation; Conformational analysis; Selective 2D *J*-δ INEPT NMR spectroscopy; Monte Carlo simulation

1. Introduction

Hyperacute rejection, a phenomenon during the discordant xenotransplantation of an organ from a pig to a primate, is triggered by the binding of the naturally occurring antibodies to the antigens expressed on the xenograft cells [1,2]. This results in the destruction of the vascular endothelium of the donor organ within minutes. Similar to the destruction of red blood cells in ABO-mismatched organ allotransplants, the major antigen against the human natural antibodies on porcine endothelium has been identified as linear carbohydrate structures bearing an α-Gal-(1→3)-Gal terminus (α-Gal epitope). The human natural anti α-Gal antibodies, namely anti-Gal, can bind trisaccharides, namely α-D-Gal*p*-(1→3)-β-D-Gal*p*-(1→4)-β-D-Glc*p* (**1**) and α-D-Gal*p*-(1→3)-β-D-Gal*p*-(1→4)-β-D-GlcNAc*p* (**2**), and the pentasaccharide, α-D-Gal*p*-(1→3)-β-D-Gal*p*-(1→4)-β-D-GlcNAc*p*-(1→3)-β-D-Gal*p*-(1→4)-β-D-Glc*p* (**3**) [3].

* Corresponding author. Tel.: +1-313-9936759; fax: +1-313-5775831.

E-mail address: pwang@chem.wayne.edu (P.G. Wang)

0008-6215/99/$ - see front matter
PII: S0008-6215(98)00321-8

Such α-Gal epitopes are synthesized by a unique enzyme α-(1→3) galactosyltransferase [α-(1→3)-GalT, EC 2.4.1.151] that is expressed in most mammals, except human and other Old World primates. The enzyme mediates the transfer of galactose from uridine diphosphate galactose to *N*-acetyllactosamine containing oligosaccharides and glycolipids. In contrast, anti-Gal is found only in humans and other Old World primates [4]. It is a natural polyclonal antibody comprising 1–2% of total human IgG and 3–8% IgM [1b]. The binding of anti-Gal to α-Gal epitopes expressed on glycolipids and glycoproteins of xenograft cells (e.g., porcine cells) induces antibody-dependent cell-mediated cytotoxicity by human blood monocytes and macrophages [5] and complement-mediated lysis of the xenograft cells [6]. The α-(1→3) linkage at the nonreducing end of α-Gal epitopes is believed to be the major structural motif that triggers the hyperacute rejection through α-Gal/anti-Gal interaction upon xenotransplantation. The remaining parts of the carbohydrate sequences at the reducing end are considered only to enhance the binding to the antibodies [7]. Hence, determination of the solution conformations of α-galactosyl epitope, especially the α-(1→3) linkage, provides the structural basis for antibody recognition. Conformational investigations have been performed on α-D-Gal*p*-(1→3)-β-D-Gal*p* disaccharide sequence using 1D NOE (nuclear Overhauser effect) [8], ^{13}C chemical shifts [9], as well as molecular modeling [10,11]. In addition, conformational studies of isoglobotriaosylceramide, which contains a linear α-D-Gal*p*-(1→3)-β-D-Gal*p*-(1→4)-β-D-Glc*p* trisaccharide sequence were carried out in nonaqueous media [12]. However, no detailed conformational analysis of α-Gal epitopes has been reported. Recently, we have achieved an efficient enzymatic synthesis of α-Gal oligosaccharides using a recombinant α-(1→3)-GalT [13]. In this paper, we report conformational analysis of a water-soluble, synthetic *N*-linked α-D-Gal*p*-(1→3)-β-D-Gal*p*-(1→4)-β-D-Glc*p* trisaccharide epitope **4** (Fig. 1).

In this analysis, complete ^{1}H and ^{13}C NMR spectra were first assigned, followed by the determination of each monosaccharide residue and hydroxymethyl exocyclic group conformations. Three-bond heteronuclear long-range coupling constants $^{3}J_{CH}$ and NOEs from interglycosidic residues were measured and compared with ensemble average data. The flexibility and dynamics of the α-(1→3)-linkage were evaluated by temperature-dependent interglycosidic long-range coupling constants ($^{3}J_{CH}$) obtained from NMR measurements and molecular modeling. The resulting conformational features of the α-Gal epitope will aid the design of improved α-Gal mimetics that may be useful in reducing hyperacute rejection during xenotransplantation.

2. Results and discussion

^{1}H and ^{13}C assignments.—The ^{1}H NMR spectrum of **4** at 22 °C in D_2O showed unresolved overlapped resonances between 3.6 and 4.3 ppm. We carried out the measurement at 40 °C and obtained better resolution and separation for the proton resonances. Consequently, we acquired all NMR experiments at 40 °C to facilitate the resonance assignments. The proton chemical shifts and coupling constants of the α-Gal and β-Glc spin systems were established in a straightforward manner

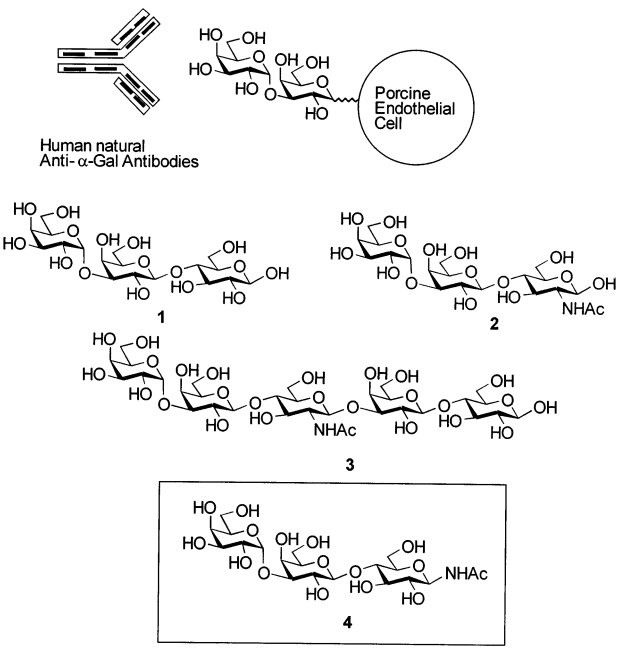

Fig. 1. The interaction of α-Gal/anti-Gal causes hyperacute rejection in xenotransplantation.

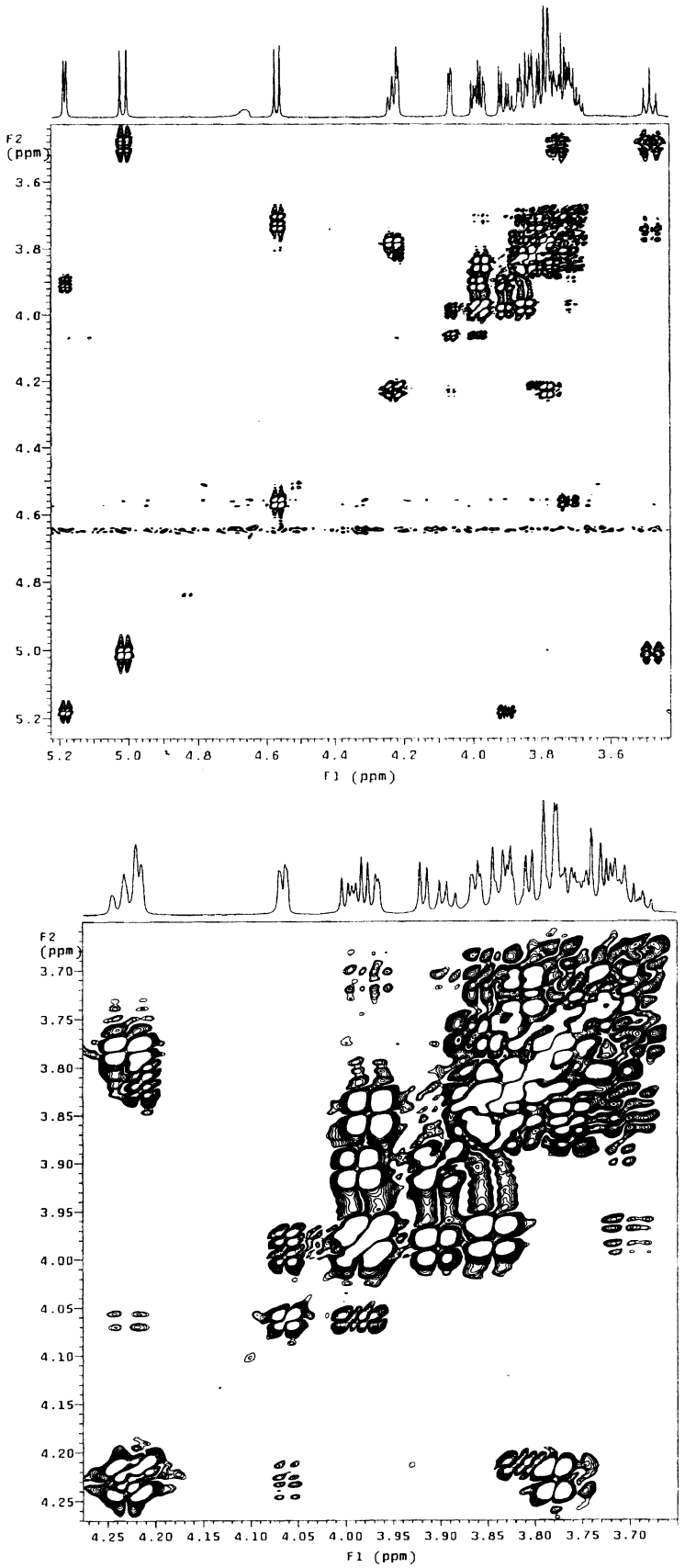

Fig. 2. DQF-COSY spectra and expanded region between 3.60 and 4.30 ppm of α-Gal epitope **4**.

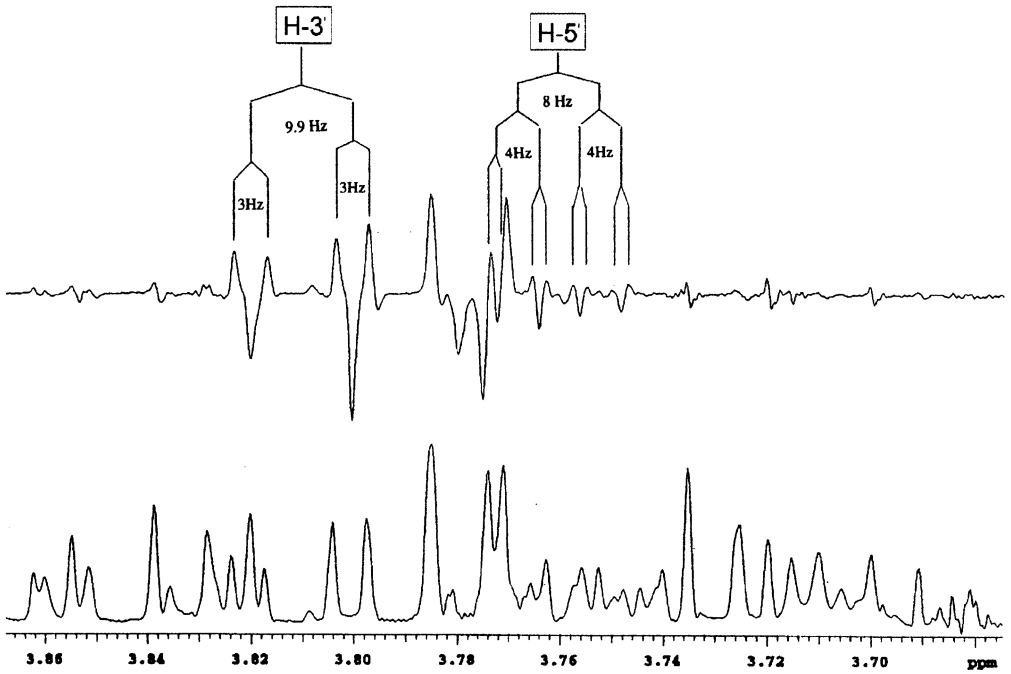

Fig. 3. Homodecoupling difference spectrum obtained by irradiating H-4′ of β-Gal.

by locating the anomeric proton resonances and walking through the cross-peaks in the DQF-COSY (double quantum filtered correlated spectroscopy) [14] (Fig. 2), and by TOCSY (total correlation spectroscopy) [15], and further confirmed with 1D TOCSY [16] spectra. However, this strategy was only successful in providing the proton connectivity of H-1′ to H-4′ of the β-Gal spin system. The assignment of H-5′ of β-Gal was obtained from the difference double resonance (DDR) spectrum, upon homodecoupling irradiation of the H-4′ that showed 1 Hz coupling to H-5′ at 3.76 ppm and 3 Hz coupling to H-3′ at 3.81 ppm (Fig. 3). Finally, the proton coupling connectivity between H-5′, H-6a′ and H-6b′ was established by observation of cross-peaks in the DQF-COSY spectrum, which completed the proton assignments of β-Gal spin system. The assignments of all carbon signals of **4** were confirmed by DEPT, INAPT (insensitive nuclei assigned by polarization transfer) [17] and HMQC (heteronuclear multiple quantum correlation) [18] experiments (Table 1).

INAPT has been used successfully for the determination of the glycosidic linkage in a number of oligosaccharide structures [19]. In the case of three-bond, long-range coupling, selective irradiation of the anomeric proton allowed us to assign the intraresidue C-3 and C-5, and simultaneously determine the interglycosidic linkage through H–C–O–C three-bond, long-range coupling. Most of the $^{3}J_{CH}$ three-bond coupling constants across the glycosidic linkage presumably lie between 3 and 8 Hz [19]. An array of coupling constants between 3 and 12 Hz was used to set up the pulse delays, which helped to observe the sites of interglycosidic linkages. In addition, it is known that a substituent on the oxygen atom attached to any carbon of the sugar affects the chemical shift of that carbon atom, moving it downfield by 5–11 ppm [20]. The ^{13}C signals for C-3′ of β-Gal and C-4 of Glc were deshielded by 5–8 ppm when compared to those of the corresponding hydroxy-substituted carbon atoms. This indicated the presence of $1\rightarrow3$ and $1\rightarrow4$ linkages in **4**. Simultaneously, the accurate assignments of C-5s in Gal residues using INAPT, followed by the high-resolution HMQC spectrum, verified the corresponding H-5s assignments obtained previously from 1D TOCSY and DDR spectra. The complete data of $^{3}J_{HH}$ scalar coupling constants were compared to the the-

Table 1
^{1}H and ^{13}C NMR spectral data for compound **4** at 313 K[a]

	Chemical shifts (ppm) and coupling constants (Hz)					
	α-Gal		β-Gal		β-Glc	
	H	C	H	C	H	C
1	5.19 d(3.9)	96.377	4.57 d(7.8)	103.675	5.01 d(9.1)	79.973
2	3.91 dd(10.3,3.9)	69.064	3.72 dd(7.8,9.8)	70.43	3.49 t(9.1)	72.344
3	3.995 dd(10.3,3.2)	70.187	3.81 dd (9.9,3)	78.208	3.76 dd(7.8,9.1)	75.98
4	4.06 dd(3.2,1.2)	70.032	4.21 dd(3,1)	65.763	3.73 t(7.8)	79.065
5	4.23 td(5.7,1.2)	71.716	3.76 ddd(8,4,1)	75.89	3.68 ddd(7.8,4,1.9)	77.18
6	3.78 d(6.5)	61.81	3.82 dd(4,11.8) 3.86 dd(11.8,8.1)	61.81	3.85 dd(12.2,4) 3.98 dd(12.2,1.9)	60.881

[a] ^{1}H and ^{13}C NMR chemical shifts are offset by +0.04 and −2.00 ppm, respectively, when referenced to TSP.

oretical vicinal proton–proton coupling constants predicted by HLA empirical equations [21]. It was confirmed that α-Gal, β-Gal and Glc residues were all in the $^4C_1$ chair conformations.

Conformational distribution about the exocyclic C-5–C-6 bond.—Rotational populations of primary hydroxyl groups on each residue of this trisaccharide **4** were studied. All the possible rotamers of the Gal residue are shown in Fig. 4.

Analysis of the rotational population relies on obtaining $^3J_{5,6R}$ and $^3J_{5,6S}$ coupling constants that have the relationship with H-5–C-5–C-6–H-6 dihedral angles through a modified Karplus equation [21]. Assignment of H-6R and H-6S resonances in the β-Gal residue is illustrated in Fig. 5. We observed the NOE contact between Gal H-4′ and H-6′ at 3.82 ppm (high field), while there was no NOE between Gal H-4′ and H-6′ at 3.86 ppm (low field). The large $^3J_{5,6}$ coupling constants (8.1 Hz at 3.86 ppm) allowed us to assign the H-6′ at 3.86 ppm (low field) as H-6R and H-6′ at high field as H-6S. For the hydroxymethyl group in β-Glc, we assigned them according to the general features of δ H-6S > δ H-6R and $^3J_{5,6R}$ (ca. 5–6 Hz) > $^3J_{5,6S}$ (ca. 2 Hz) as in the previous studies on D-glucose and its derivatives [12a,22]. It is worth mentioning that Ohrui and co-workers assigned H-6R and H-6S protons using a stereospecific deuteration method [22].

Our results indicated that the primary hydroxymethyl groups of the α-Gal, β-Gal, and β-Glc residues adopted predominantly *tg*, *gt*, and *gg* orientations in trisaccharide **4**, respectively (Table 2). The *tg* orientation for Glc was rarely occupied, but it was the most populated conformer for the terminal α-Gal. For β-Gal, an intramolecular hydrogen bonding formation between OH-6 and the ring oxygen presumably contributed to the predominance of *gt* orientation. Such conformational preference for glucose and galactose residues was also observed in previous studies [24]. As a result, the preferred conformations about the C-5–C-6 bond in each sugar residue may provide some important information for the design of α-Gal epitope mimetics.

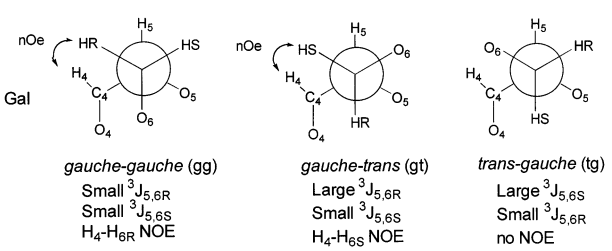

Fig. 4. Primary hydroxyl group conformations in Gal residue.

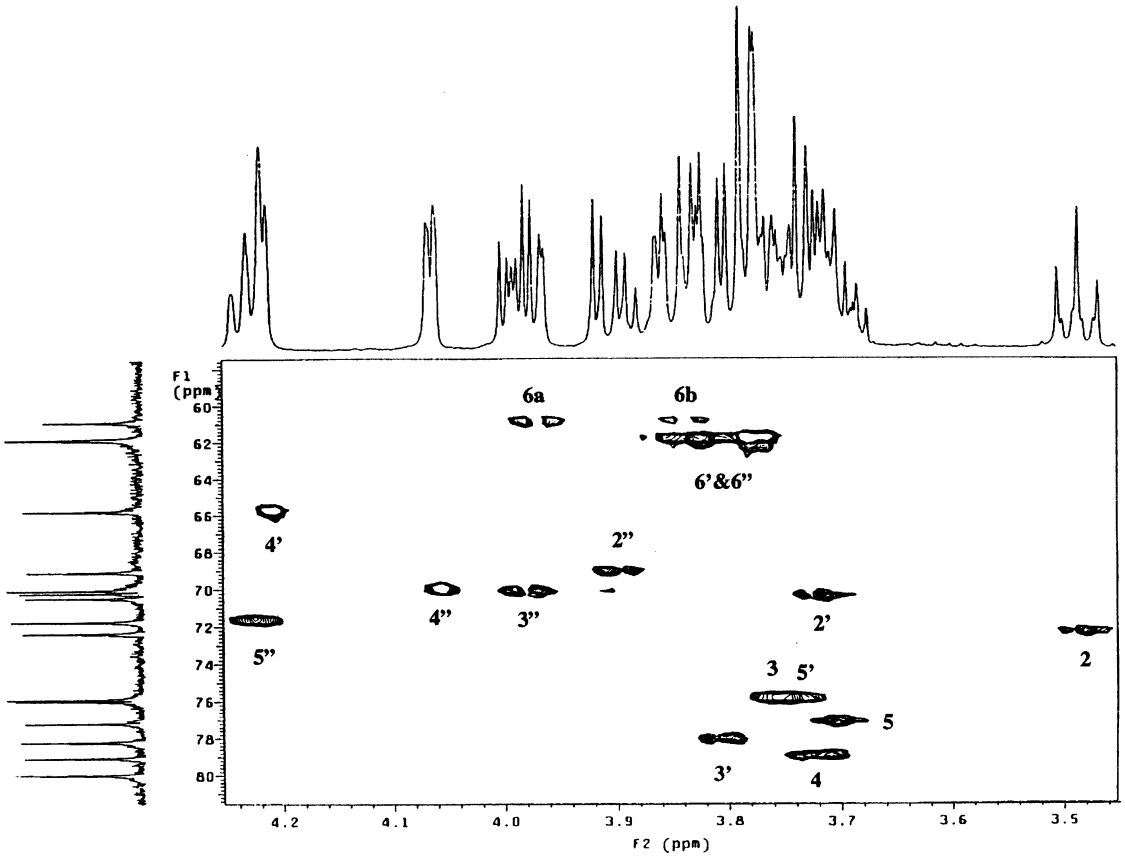

Fig. 5. Expanded region of $^{13}C-^{1}H$ correlation of α-Gal epitope **4** from HMQC experiment.

Glycosidic linkage conformations.—A selective 2D *J*-δ INEPT experiment [25] was used for measuring the three-bond, long-range proton–carbon coupling constant, $^{3}J_{CH}$, which has attracted considerable attention for the conformational analysis of flexible oligosaccharides over the past few years [26]. This approach allowed unequivocal detection of doublets for each carbon that is three-bond, long-range coupled with the selected proton. The experiment was optimized for polarization transfer through 5 Hz coupling. The spectral width was adjusted to find a best compromise between resolution and signal-to-noise ratio. The coupling constants of $J_{H1''-C1''-O-C3'}$ and $J_{H1'-C1'-O-C4}$ were readily determined through the polarization transfer from the well-isolated anomeric protons. The measuring of the coupling constant $J_{H3'-C3'-O-C1''}$ required selective irradiation of H-3′ of β-Gal, which was overlapped with other protons. Close inspection of the HMQC spectra (Fig. 5) revealed that the only interfering proton was one of the H-6′ of β-Gal. The 2D *J*-δ INEPT spectra for an α-(1→3) linkage are shown in Fig. 6. The $^{3}J_{CH}$ long-range coupling constants measured for both α-(1→3) and β-(1→4) linkages are listed in Table 3.

Table 2
$^{3}J_{5,6R}$ and $^{3}J_{5,6S}$ coupling constants for compound **4** and calculated population ratios[a] for staggered rotamers

	$^{3}J_{5,6R}$ (Hz)	$^{3}J_{5,6S}$ (Hz)	*gg*%	*gt*%	*tg*%
α-Gal	6.5	6.5	23	31	46
β-Gal	8.1	4.0	22	59	19
β-Glc	4.0	1.9	73	25	2

[a] Population ratios obtained from the following equations [22,23]: (1) $1.3gg+2.7gt+11.7tg = {}^{3}J_{5,6S}$, (2) $1.3gg+11.5gt+5.8tg = {}^{3}J_{5,6R}$ and (3) $gg+gt+tg = 1$.

The rigidity of the glycosidic linkage can be deduced from the temperature dependence of the long-range $^{3}J_{CH}$ coupling constants [27]. The interglycosidic $^{3}J_{CH}$ coupling constants for the α-(1→3) linkages were measured at three different temperatures by using selective 2D *J*-δ INEPT experiments with the final resolution in the f_1 [*J* (C, H)] of 0.15–0.19 Hz

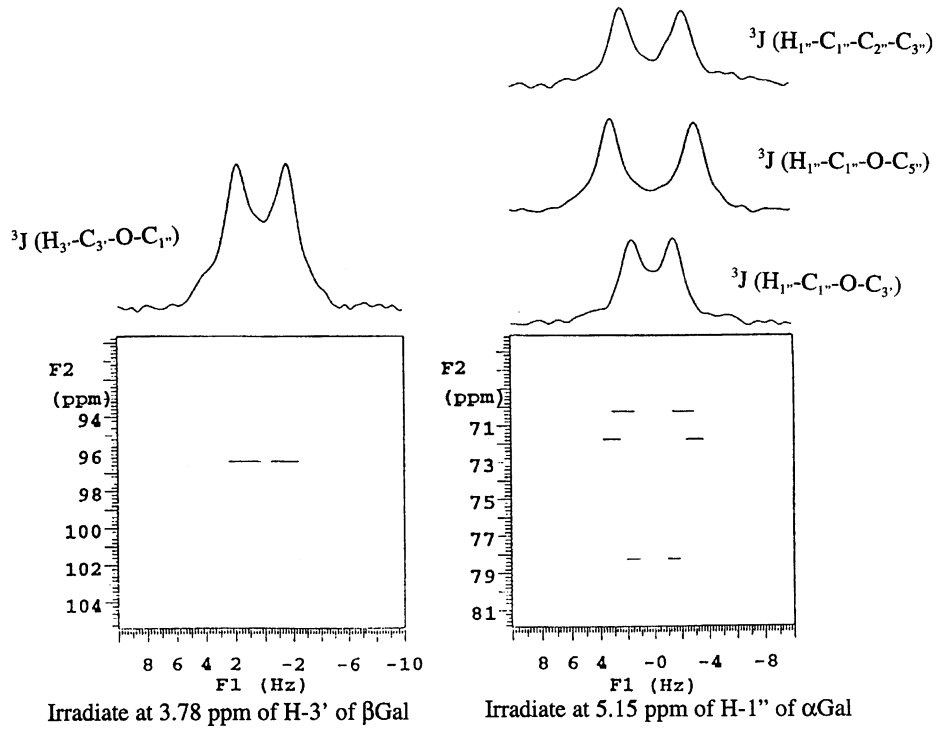

Fig. 6. Selective 2D J-δ INEPT spectra and cross sections of the α-(1→3) linkage for α-Gal epitope **4**.

per point (Table 4). The $J_{H1''-C1''-O-C3'}$ coupling constants at 295, 313 and 333 K in D_2O were measured between 2.9 and 3.1 Hz, and the corresponding $J_{H3'-C3'-O-C1''}$ were found between 3.3 and 3.4 Hz. The data provided evidence for the rigidity of the α-(1→3) linkage. The intraresidue $^3J_{CH}$ coupling constants for α-Gal were also obtained in the same 2D experiments at different temperatures (Table 5). They indicated that the NMR-derived average dihedral angles were almost independent of the temperature changes.

Interresidue NOEs were also determined to substantiate the structural information obtained from long-range coupling constant measurements. In a 1D NOE difference experiment, anomeric protons H-1″ and H-1′ of α- and β-Gal residues were irradiated, respectively. The salient NOEs for H-2″, H-3′ and H-4′ were observed upon the irradiation of the nonreducing anomeric proton (Fig. 7). However, due to the overlapping of the H-4 of Glc residue with other protons, no conclusive interresidue NOEs were obtained upon irradiation of anomeric H-1′ of β-Gal. Comparing to the previous results of NMR study of α-D-Gal*p*-(1→3)-β-D-Gal*p* disaccharide [8], consistent NOE data were obtained from the irradiation of anomeric H-1″ of the α-Gal residue. Consequently, the presence of the reducing-end residue of Glc in this case should not affect the preferential conformation of the nonreducing α-(1→3) linkage.

Conformational calculations.—Due to the flexible nature of oligosaccharides, structural and dynamic properties can hardly be defined unambiguously by evaluating the ensemble-averaged NMR data alone. Computational protocols [28], therefore, have been developed and employed to calculate experimentally accessible NMR parameters as well as to simulate internal motions that can truly reproduce the corresponding ensemble-average properties. Here we used the GEGOP program [29], which employs a modified version of the HSEA force field [30] and a Metropolis Monte Carlo (MMC) stochastic simulation procedure [31]. The HSEA/MMC protocol has been successfully applied to explore the conformational space of oligosaccharides. Ensemble-averaged values derived from this calculation have shown good agreement with time-averaged experimental data from NMR spectroscopy [32].

In the molecular modeling calculation, each pyranose ring structure was kept rigid. The

Table 3
Interglycosidic coupling constants $^3J_{CH}$ (Hz) for compound **4** measured at 313 K

ϕ (H-1″–C-1″–O–C-3′)	ψ (H-3′–C-3′–O–C-1″)	ϕ (H-1′–C-1′–O–C-4)
3.1	3.4	3.6

conformations of the oligosaccharide were defined by dihedral angles of glycosidic linkage (ϕ and ψ), the exocyclic H-5–C-5–C-6–H-6 torsional angle (ω) and glycosidic bond angle (τ). The global minimum conformation of α-D-Gal*p*-(1→3)-β-D-Gal*p*-(1→4)-β-D-Glc*p* (**1**) was obtained by performing the potential energy minimization with the GEGOP program. The global minimum conformation was located around $\phi/\psi = -50°/-34°$ and 52°/4° for the corresponding α-(1→3) and β-(1→4) linkages. Because the α-(1→3) linkage of the trisaccharide is of more importance in the antibody recognition, a grid search of the dihedral angles ϕ and ψ around this linkage versus energy was performed to locate all the local minima in the conformational space. An energy contour map with energy up to 10 kcal/mol was obtained for the α-(1→3) linkage (Fig. 8). The potential energy well around A, the global minimum, was found to be broad and shallow. A distinct local minimum B was observed at $\phi/\psi = -25°/-178°$. The overall appearance of this energy contour map was similar to the relaxed maps of α-D-Gal-(1→3)-D-Gal calculated by an MM3 [10a] and a general-purpose MM2 force field [10b]. However, a third minimum at −40°/60° was reported in their studies. In our calculations using rigid pyranose ring geometry, this region was an extension of the global minimum A. For the following calculation interests, this region was also labeled as minimum C on the map.

Furthermore, MMC simulations were employed to sample populations of accessible conformations. In this case, the flexibility and dynamics of the α-(1→3) linkage conformation were also studied. As shown by Pinto and co-workers, the MMC simulations were found to be a reasonably good model in predicting carbohydrate conformational transitions over molecular dynamics simulations [33]. The MMC simulations were conducted at 300 and 800 K with 100,000 macro steps, respectively. Each macro step was defined as a complete sweep of all the variables in the molecule [32b]. Scatter plots representing the probability of the accessible glycosidic torsional angles were employed to delineate a two-dimensional ϕ/ψ dihedral angle population map from a multidimensional hyperspace (Fig. 9). The 1D projections of the populations are shown at the top and left of the scatter plots. Only a small portion of the conformational space was sampled near the global minimum A when the calculation was carried out at 300 K. No populations were observed in the regions of B and C. In order to uniformly sample the conformational space, a higher temperature parameter of 800 K was employed. Although this temperature was normally enough to sample the whole conformational space [32a], no interconversion was observed between regions A and B. Obviously, the energy barrier between A and B was too high to surmount. Nevertheless, the elevated temperature increased the population by overcoming the surrounding energy barriers within 10 kcal/mol to reach region C as compared to a grid search contour map. The scatter plots generated from MMC at 300 and 800 K were found to be superimposable to the global minimum A. In order to locate the other local minimum B, a Monte Carlo simulated annealing approach was used. Starting from 2000 K to surmount all the energy barriers, the system

Table 4
Interglycosidic coupling constants $^3J_{CH}$ (Hz) for the α-(1→3) linkage in compound **4** measured at different temperatures

T (K)	293	313	333
$J_{H1''–C1''–O–C3'}$ (Hz)	2.9	3.1	3.0
$J_{H3'–C3'–O–C1''}$ (Hz)	3.3	3.4	3.4

Table 5
Intraresidue $^3J_{CH}$ (Hz) for α-Gal in compound **4** measured at different temperatures

T (K)	293	313	333
$J_{H1''–C1''–C''–C3''}$ (Hz)	4.4	4.6	4.5
$J_{H1''–C1''–O–C5''}$ (Hz)	6.1	6.2	6.3

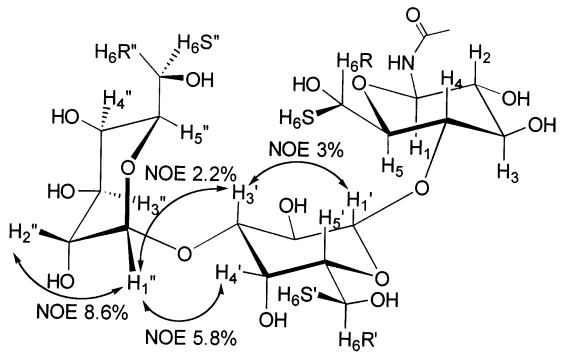

Fig. 7. Observed NOEs in compound **4**.

was then 'cooled' down every 50 steps to 300 K and was eventually trapped in the other local minimum. We can see in Fig. 10 that the scatter plot gave out the dot distribution around $\phi/\psi = -25°/-178°$, which resembled the energy grid search contour map. The simulated annealing confirmed that local minimum B does exist along with the other two minima.

The temperature dependence on $^3J_{CH}$ coupling constants was investigated by MMC simulation at 300, 400 and 800 K. The resulting glycosidic torsional angles from the MMC simulation were transformed into the ensemble-averaged, three-bond heteronuclear long-range coupling constants $\langle J_{H1''-C1''-O-C3'}\rangle$ and $\langle J_{H3'-C3'-O-C1''}\rangle$ using a modified Karplus equation: $^3J_{CH} = 5.7\cos^2\psi - 0.6\cos\psi + 0.5$ [34] (Table 6). It is noteworthy that $\langle J_{H1''-C1''-O-C3'}\rangle$ and $\langle J_{H3'-C3'-O-C1''}\rangle$ were in good agreement

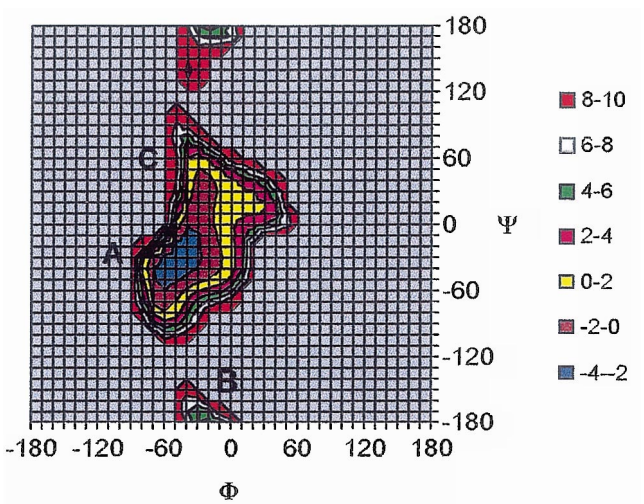

Fig. 8. Energy grid map of the α-(1→3) linkage in compound **1**. Isoenergy contours are scaled at 2 kcal/mol intervals up to 10 kcal/mol above the global minimum energy.

with the experimental data in Table 4, as even the calculation was simplified without using an *N*-acetyl group in the trisaccharide and without taking hydrogen-bonding terms into account. The calculated interglycosidic coupling constants were not temperature sensitive, indicating a restricted flexibility of the α-(1→3) glycosidic linkage.

MMC simulation at 800 K showed excellent agreement with experimental $^3J_{CH}$ coupling constants. The dihedral angles with the highest population, smallest and largest values, angle range, and populations for other family of conformers in α-(1→3) and β-(1→4) linkages at 800 K are listed in Table 7. According to the occurrence of dihedral angles in MMC calculation, the ϕ/ψ population for an α-(1→3) linkage showed the highest population at $-48°/-36°$, which was located in global minimum A. A range of 136° about this conformation was significantly populated in the ϕ dimension. A wider range was populated between -106 and 101° in the ψ dimension. A broad lightly populated area was centered at $-36°/54°$, which was located in a local minimum C, and accounted for 11% of the total population. As for the β-(1→4) linkage, the highest population was found at 54°/0°. The second family of conformers was located at 168°/6° with a population of 1.5%. This linkage has been well defined by a number of standard force fields in all relaxed approaches [35]. Our MMC calculation using rigid pyranose rings was in good agreement with the previous calculations based on the MM3* and CVFF force fields. The ranges over which the dihedral angles ϕ (H-1″–C-1″–O–C-3′) and ϕ (H-1′–C-1′–O–C-4) varied indicated that the rotation of the α-(1→3) linkage near the anomeric position was more restricted than that of a β-(1→4) linkage.

The MMC calculations indicated that the exocyclic torsional angles of ω (O-5–C-5–C-6–O-6) were more flexible than the interglycosidic dihedral angles. It was also found that the primary hydroxyl group on the α-Gal terminus was more flexible than that of the β-Gal residue. The starting angles were −140° (*tg* conformation) in all cases. The sampling at 300 K resulted in rotational

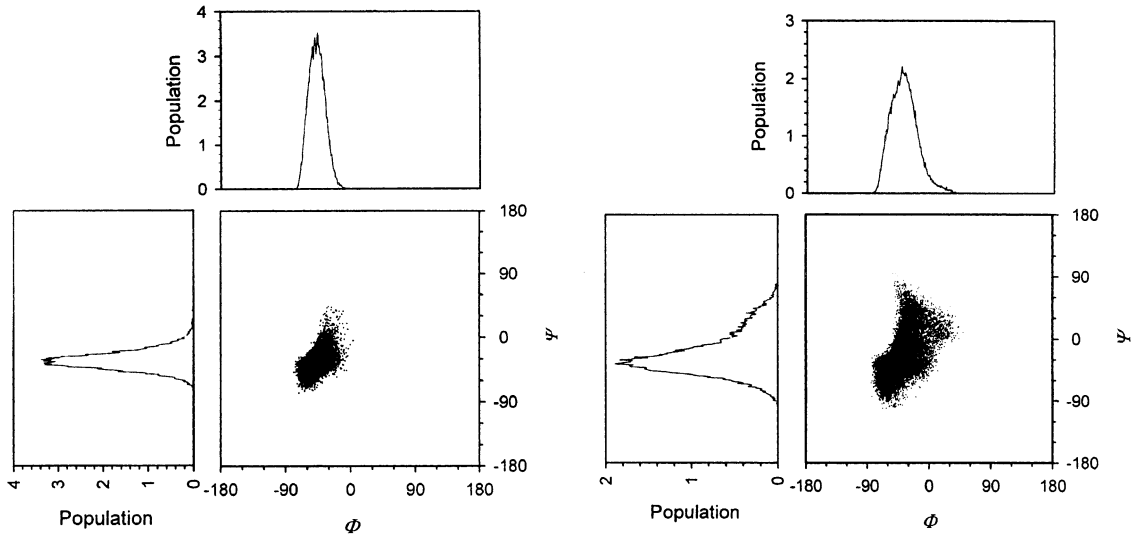

Fig. 9. Scatter plots of the α-(1→3) linkage at 300 K (left) and 800 K (right) resulting from MMC simulations. 1D projections of the probability of populated torsional angles (%) are shown at the top and left of the scatter plots.

populations of 21/72/7% (*gg*/*gt*/*tg*) for α-Gal, 17/83/0% (*gg*/*gt*/*tg*) for β-Gal, and 62/37/1% (*gg*/*gt*/*tg*) for β-Glc. The calculation was in good agreement with experimental results shown in Table 2, indicating a high percentage of *gg* in β-Glc and *gt* in β-Gal.

Steady-state NOEs were calculated according to a full relaxation matrix option [36] provided from the GEGOP program. The ensemble-average NOEs at 800 K were compared to the experimentally determined time-averaged values. Relative NOEs were applied by setting the H-1″–H-2″ intraglycosidic NOE at 1.0. The results in Table 8 clearly indicate that the theoretical NOE values were consistent with the experimental data (Fig. 11).

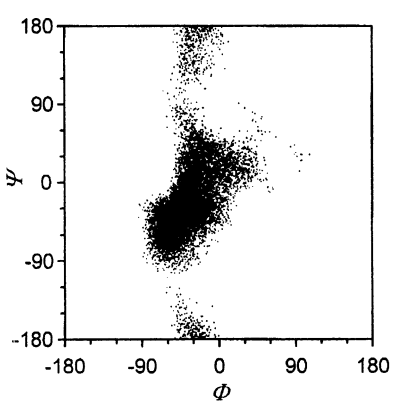

Fig. 10. Scatter plot of Monte Carlo simulated annealing starting from 2000 K.

3. Experimental

NMR experiments.—A solution containing 38 mg of trisaccharide **4** was dissolved in 0.6 mL of D_2O. ^1H and ^{13}C NMR spectra at 22, 40 and 60 °C were assigned by a combined use of 1D and 2D standard techniques on a Varian Unity 500 NMR spectrometer. Internal sodium 3-(trimethylsilyl)propionate (TSP) was used. All NMR spectra at 40 °C were offset by +0.04 ppm in the proton dimension and −2.00 ppm in the carbon dimension when referenced to TSP. All NMR data were acquired and processed by using Varian 5.1A software. All phase-sensitive 2D NMR experiments were measured using hypercomplex protocol. Linear prediction was used in the processing of 2D phase-sensitive experiments. Presaturation of the HDO peak was performed using either transmitter presaturation in case of DQF-COSY, TOCSY and HMQC, or a Gaussian pulse in the 1D TOCSY experi-

Table 6
Interglycosidic coupling constants $\langle {}^3J_{CH} \rangle$ (Hz) for the α-(1→3) linkage calculated from MMC simulations at different temperatures

T (K)	300	400	800
$\langle J_{H1''-C1''-O-C3'} \rangle$ (Hz)	2.6	2.8	3.2
$\langle J_{H3'-C3'-O-C1''} \rangle$ (Hz)	3.8	3.8	3.7

Table 7
Torsional angles with highest population, smallest and largest values, angle ranges, and % population of the other family of conformers for α-(1→3) and β-(1→4) linkages from MMC simulations at 800 K

Linkage	Highest pop.	Smallest	Largest	Range	Pop. 2nd (%)
ϕ (H-1″–C-1″–O–C-3′)	−48 (−36)[a]	−86	50	136	11[b]
ψ (H-3′–C-3′–O–C-1″)	−36 (54)	−106	101	207	
ϕ (H-1′–C-1′–O–C-4)	54 (168)	−56	−169	247	1.5
ψ (H-4–C-4–O–C-1′)	0 (6)	−92	56	148	

[a] Values in parentheses are for the second conformer.
[b] Population was calculated between 18 and 96° in the ψ dimension, and between −6 and −48° in the ϕ dimension.

ment. The DQF-COSY phase-sensitive experiment was performed using spectral width of 1200 Hz to obtain 128 FIDs with 512 data points in the f_2 and four scans each. The repetition rate was 1.7 s. The FIDs were processed using the Gaussian function after zero filling to 8k in both dimensions. TOCSY spectra were recorded using the MLEV-17 multipulse decoupling sequence with a total mixing time of 150 ms. A total of 372 FIDs were collected with 1024 data points and 16 scans per t_1 increment. The spectral width was 1100 Hz. The repetition rate was 1.7 s. The data were transformed as a 4k × 4k matrix with the Gaussian function applied on both dimensions. The one-bond carbon-proton shift correlation spectrum was obtained in the ^{1}H-detected mode by HMQC experiments. The proton spectral width was 1200 Hz, and the carbon-13 spectral width was 7500 Hz. The repetition rate was 1.2 s. The ^{1}H–^{13}C one-bond coupling constant was set at 150 Hz. A total of 360 FIDs were collected using 1k data points. Zero filling was set to 8k in f_2 and 4k in f_1. The Gaussian window function was applied to both dimensions. 1D TOCSY spectra were processed in an absolute-value mode. The anomeric proton resonance of each sugar residue was selectively inverted. The spectral width was 8297 Hz. The repetition rate was 2.9 s. Each FID was acquired in 32k data point with 240 scans. The MLEV-17 mixing times were incremented from 50 to 200 ms in 50 ms increments. Selective 2D J-δ INEPT experiments performed on the α-(1→3) linkage were described as follows: for irradiating 5.19 ppm at H-1″ on α-Gal at 40 °C, the repetition rate was 1.26 s. The refocusing interval was 50 ms. The ^{13}C spectral width was 1974 Hz, and the ^{1}H spectral width was 20 Hz. A total of 26 FIDs were collected with 768 scans per t_2. Each scan was acquired in 1k data points. The FIDs were processed by using the Gaussian function after zero filling to extend the data matrix to 4096 × 106. The final resolution was 0.19 Hz per point in the f_1 [J (C, H)] dimension. For irradiating 3.82 ppm at H-3′ on β-Gal at 40 °C, the repetition rate was 1.26 s. The refocusing interval was 50 ms. The ^{13}C spectral width was 1967 Hz, and the ^{1}H spectral width was 20 Hz. A total of 31 FIDs were collected with 576 scans per t_2. Each scan was acquired in 1k data points. The FIDs were processed by using the Gaussian function after zero filling to extend the data matrix to 4096 × 124. The final resolution was 0.16 Hz per point in the f_1 [J (C, H)] dimension. For 1D NOE difference spectroscopy used in steady-state experiments, saturation of the signals was accomplished by single line irradiation for 6.0 s. The repetition rate was 8.9 s. Each FID was acquired in 32 scans.

Conformational calculations.—The conformational calculations were performed on a Silicon Graphics Iris workstation. A modified

Table 8
Relative NOE values for α-D-Gal*p*-(1→3)-β-D-Gal*p*-(1→4)-β-D-Glc*p*

Proton satd	Proton obsd	Experiment[a]	$\langle$NOE$\rangle_{MMC}$[b]
H-1″	H-2″	1.00	1.00
	H-3′	0.26	0.26
	H-4′	0.67	0.44

[a] Experimental results obtained at 40 °C for compound **4**.
[b] Average NOE values calculated for α-D-Gal*p*-(1→3)-β-D-Gal*p*-(1→4)-β-D-Glc*p* at 800 K.

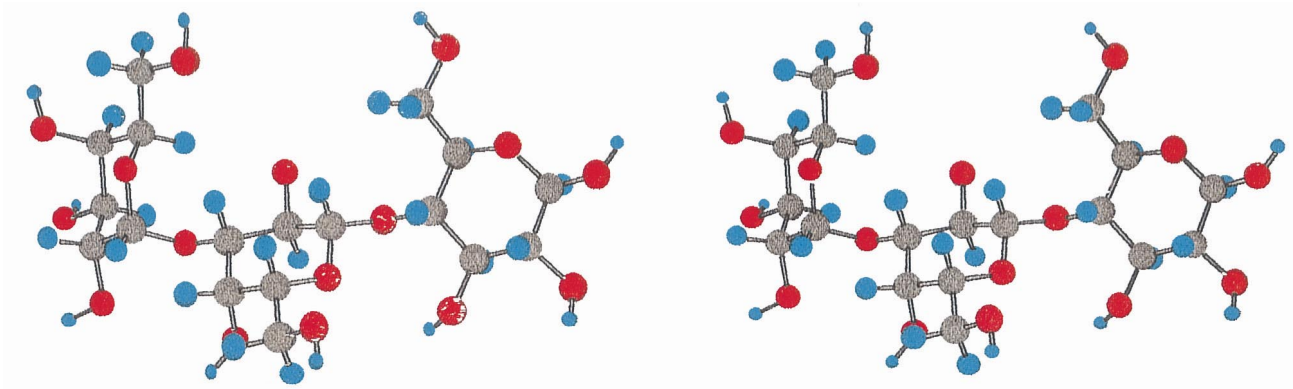

Fig. 11. Stereoview representation of the lowest energy conformation of the α-Gal trisaccharide epitope.

HSEA force field was applied, which only took into account the nonbonded interaction, as well as the exo-anomeric effect. Minimization, grid search and MMC calculations were performed using the GEGOP program. The atomic coordinates of the each monosaccharide residue was taken from either X-ray or neutron-diffraction studies. Each residue was treated as a rigid entity: only dihedral angles (ϕ and ψ) between interglycosidic residues, exocyclic H-5–C-5–C-6–H-6 torsional angles (ω) and the glycosidic bond angle (τ) were allowed to move. Recent studies by Kopper and Meyer [32e] and Pérez and co-workers [32g] have shown that, although measurable improvement has been found by relaxing the ring geometry in the study of intraglycosidic NOEs, it is safe to keep the chair conformation of pyranose ring during the entire calculation when it is to study the flexibility of the glycosidic linkages. Grid search of trisaccharide **1** at the α-(1→3) glycosidic linkage was performed as a two-dimensional search, varying dihedral angles ϕ and ψ in steps of 10°, covering a range of 360°. Energy minimization of each grid was done by holding the two dihedral angles constant while optimizing the rest of variables. MMC calculations were performed with the temperature set to 300, 400, 800 and 2000 K. The number of performed MMC macro steps was 100,000 with maximum step lengths of 20.0° (ϕ and ψ), 24.0° (ω), 28.0° (dihedral angles of hydroxyl groups) and 3.0° (τ), resulting in the acceptance ratios of 30–60% for new conformations. The steady-state NOEs were calculated according to a full relaxation matrix option assuming isotropic motion with molecular tumbling correlation time (τ_c) of 0.1 ns and no external relaxation effects. Ensemble-averaged $\langle$NOE$\rangle$ data were obtained by sampling the $\langle r^{-6}\rangle$ at 300 K.

Acknowledgements

The work was generously supported by research grants from NIH (GM54074), NSF (BES-9728366), ACS-PRF (301616-G1), the American Cancer Society, FL Division (F95UM-2), the American Heart Association, FL Affiliate (9701760), the Mizutani Foundation (138A), the Herman Frash Foundation (449-HF97), and Hercules, Inc. for our research programs. We thank Professor J. Santa Lucia for discussions and letting us use his Silicon Graphics Iris workstation. We are much indebted to Professor Dr B. Meyer at the University of Hamburg and Professor Dr K. Bock at the Carlsberg Laboratory for providing the GEGOP programs.

References

[1] J.L. Platt, *Nature*, 392 (1998) 11–17 (Suppl.).
[2] R.P. Rother, S.P. Squito, *Cell*, 86 (1996) 185–188.
[3] (a) D.K.C. Cooper, E. Koren, R. Oriol, *Immunol. Rev.*, 141 (1994) 31–58. (b) U. Galili, *Immunol. Today*, 14 (1993) 480–482. (c) M.S. Sandrin, H.A. Vaughan, I.F.C. McKenzie, *Transplant. Rev.*, 8 (1994) 134. (d) B.E. Samuelsson, L. Rydberg, M.E. Breimer, A. Backer, M. Gustavsson, J. Holgersson, E. Karlsson, A.-C. Uyterwaal, T. Cairns, K. Welsh, *Immunol. Rev.*, 141 (1994) 151–168.
[4] (a) U. Galili, M.R. Cark, S.B. Shohet, J. Buehler, B.A. Macher, *Proc. Natl. Acad. Sci. USA*, 84 (1987) 1369–1373. (b) U. Galili, S.B. Shohet, E. Kobrin, C.L.M. Stults, B.A. Macher, *J. Biol. Chem.*, 263 (1988) 17755–17762.

[5] U. Galili, F. Anaraki, A. Thall, C. Hill-Black, M. Radic, *Blood*, 82 (1993) 2485–2493.
[6] M. Sandrin, H.A. Vaughan, P.L. Dabkowski, I.F.C. McKenzi, *Proc. Natl. Acad. Sci. USA*, 90 (1993) 11391–11395.
[7] F. Neethling, D. Joziasse, N. Bovin, D.K.C. Cooper, R. Oriol, *Transplant. Int.*, 9 (1996) 98–101.
[8] R.U. Lemieux, K. Bock, L.T.J. Delbaere, S. Koto, V.S. Rao, *Can. J. Chem.*, 58 (1980) 631–653.
[9] K. Bock, A. Brignole, B.W. Sigurskjold, *J. Chem. Soc., Perkin Trans. 2*, (1986) 1711–1713.
[10] (a) A. Imberty, E. Mikros, J. Koca, R. Mollicone, R. Oriol, S. Pérez, *Glycoconjugate J.*, 12 (1995) 331–349. (b) C.A. Stortz, A.S. Cerezo, *J. Carbohydr. Chem.*, 13 (1994) 235–247.
[11] F. Bizid, I. Tvaroska, *Chem. Pap.*, 49 (1995) 202–214.
[12] (a) L. Poppe, J. Dabrowski, C.-W. Von der Lieth, K. Koike, T. Ogawa, *Eur. J. Biochem.*, 189 (1990) 313–325. (b) J. Dabrowski, K. Trauner, K. Koike, T. Ogawa, *Chem. Phys. Lipids*, 49 (1988) 31–37.
[13] J. Fang, J. Li, X. Chen, Y. Zhang, J. Wang, Z. Guo, W. Zhang, L. Yu, K. Brew, P.G. Wang, *J. Am. Chem. Soc.*, 120 (1998) 6635–6638.
[14] U. Piantinis, O.W. Sorensen, R.R. Ernst, *J. Am. Chem. Soc.*, 104 (1982) 6800–6801.
[15] L. Braunschweiler, R.R. Ernst, *J. Magn. Reson.*, 53 (1983) 521–528.
[16] H. Kessler, H. Oschkinat, C. Griesinger, *J. Magn. Reson.*, 70 (1986) 106–133.
[17] (a) A. Bax, *J. Magn. Reson.*, 57 (1984) 314–318. (b) A. Bax, J.A. Ferretti, N. Nashed, D.M. Jerina, *J. Org. Chem.*, 50 (1985) 3029–3034.
[18] (a) L. Muller, *J. Am. Chem. Soc.*, 101 (1979) 4481–4484. (b) A. Bax, S. Subramanian, *J. Magn. Reson.*, 67 (1986) 565–569.
[19] A. Bax, W. Egan, P. Kovác, *J. Carbohydr. Chem.*, 3 (1984) 593–611.
[20] T. Usui, N. Yamaoka, Y. Okada, N. Nakanishi, H. Sugiyama, S. Seto, *J. Chem. Soc., Perkin Trans. 1*, (1973) 2425–2432.
[21] (a) C.A.G. Haasnoot, F.A.A.M. De Leeuw, C. Altona, *Tetrahedron*, 36 (1980) 2783–2792. (b) C. Altona, C.A.G. Hasnoot, *Magn. Reson. Chem.*, 13 (1980) 417–429.
[22] (a) H. Ohrui, Y. Nishida, H. Itoh, H. Meguro, *J. Org. Chem.*, 56 (1991) 1726–1731. (b) H. Ohrui, Y. Nishida, M. Watanabe, H. Hori, H. Meguro, *Tetrahedron Lett.*, 26 (1985) 3251–3254. (c) Y. Nishida, H. Ohrui, H. Meguro, *Tetrahedron Lett.*, 25 (1984) 1575–1578.
[23] (a) D.B. Davies, *Progr. NMR Spectrosc.*, 12 (1978) 135–225. (b) G.D. Wu, A.S. Serianni, R. Barker, *J. Org. Chem.*, 48 (1983) 1750–1757.
[24] K. Bock, J.O. Duus, *J. Carbohydr. Chem.*, 13 (1994) 513–543.
[25] (a) P. Ladam, J. Gharbi-Benarous, M. Piotto, M. Delaforge, J.P. Girault, *Magn. Reson. Chem.*, 32 (1994) 1–7. (b) M. Hricovíni, I. Tvaroska, D. Uhrin, G.Y. Batta, *J. Carbohydr. Chem.*, 8 (1989) 389–394. (c) T. Jippo, O. Kamo, K. Nagayama, *J. Magn. Reson.*, 66 (1986) 344–348.
[26] I. Tvaroska, F.R. Taravel, *Adv. Carbohydr. Chem. Biochem.*, 51 (1995) 15–61.
[27] M. Hricovíni, I. Tvaroska, J. Hirsch, *Carbohydr. Res.*, 198 (1990) 193–203.
[28] (a) C.-W. Von der Lieth, T. Kozar, W.E. Hull, *J. Mol. Struct.*, 395 (1997) 225–244. (b) R.J. Woods. *Glycoconjugate J.*, 15 (1998) 209–216.
[29] R. Stuike-Prill, B. Meyer, *Eur. J. Biochem.*, 194 (1990) 903–919.
[30] H. Thogersen, R.U. Lemieux, K. Bock, B. Meyer, *Can. J. Chem.*, 60 (1982) 44–57.
[31] N. Metropolis, A.W. Rosenbluth, M.N. Rosenbluth, A.H. Teller, E. Teller, *J. Chem. Phys.*, 21 (1953) 1087–1092.
[32] (a) L. Poppe, R. Stuike-Prill, B. Meyer, H. van Halbeek, *J. Biomol. NMR*, 2 (1992) 109–136. (b) T. Peters, B. Meyer, R. Stuike-Prill, R. Somorjai, J.R. Brisson, *Carbohydr. Res.*, 238 (1993) 49–73. (c) G. Grönberg, U. Nilsson, K. Bock, G. Magnusson, *Carbohydr. Res.*, 257 (1994) 35–54. (d) R. Stuike-Prill, B.M. Pinto, *Carbohydr. Res.*, 279 (1995) 59–73. (e) S. Kopper, B. Meyer, *Liebigs Ann.*, (1996) 1131–1137. (f) J.O. Duus, N. Nifantev, A.S. Shashkov, E.A. Khatuntseva, K. Bock, *Carbohydr. Res.*, 288 (1996) 25–44. (g) T. Weimar, T. Peters, S. Pérez, A. Imberty, *J. Mol. Struct.*, 395 (1997) 297–311.
[33] T. Weimar, S.L. Harris, J.B. Pitner, K. Bock, B. Pinto, *Biochemistry*, 34 (1995) 13672–13680.
[34] I. Tvaroska, M. Hricovíni, E. Petrakova, *Carbohydr. Res.*, 189 (1989) 359–362.
[35] M. Martin-Pastor, J.F. Espinosa, J.L. Asensio, J. Jimenez-Barbero, *Carbohydr. Res.*, 298 (1997) 15–49.
[36] J.H. Noggle, R.E. Schirmer, *The Nuclear Overhauser Effect*, Academic Press, New York, 1971.